# INFLUENCES OF LARGE-SCALE STRUCTURES ON SKIN FRICTION IN AN ADVERSE PRESSURE GRADIENT TURBULENT BOUNDARY LAYER

**Min Yoon**
Dept. of Mechanical Engineering
KAIST
Daejeon 34141, Korea
minyoon@kaist.ac.kr

**Jinyul Hwang**
Dept. of Mechanical Engineering
KAIST
Daejeon 34141, Korea
j.yhwang@kaist.ac.kr

**Hyung Jin Sung**
Dept. of Mechanical Engineering
KAIST
Daejeon 34141, Korea
hjsung@kaist.ac.kr

**ABSTRACT**

Direct numerical simulation (DNS) of a turbulent boundary layer (TBL) subjected to adverse pressure gradient (APG) at $Re_\tau = 834$ is performed to investigate large-scale influences on vortical motions. For comparison, DNS data of a zero pressure gradient (ZPG) TBL at $Re_\tau = 837$ is analyzed. The spanwise energy spectra of the streamwise velocity fluctuations show that the large-scale energy above $\lambda_z^+ \approx 400$ ($\lambda_z/\delta \approx 0.5$) is significantly enhanced in the APG TBL. Large-scale streamwise velocity fluctuations ($u_L$) is extracted by employing a long-wavelength-pass filter with a cut-off wavelength of $\lambda_z^+ \approx 400$. Two velocity-vorticity correlations ($\langle v\omega_z \rangle$ and $\langle -w\omega_y \rangle$), which represent the advective vorticity transport and vortex stretching, respectively, are conditionally averaged with respect to $u_L$ to explore the extension of large-scale influences on the vortical motions. The velocity-vorticity correlations are directly related to the skin friction coefficient ($C_f$). The total $C_f$ in the APG TBL is reduced by 28% from that in the ZPG TBL. The skin friction induced by $\langle v\omega_z \rangle$ and $\langle -w\omega_y \rangle$ contribute negatively and positively to the total $C_f$ respectively. In the APG TBL, the negative contribution of $\langle v\omega_z \rangle$ decreases 29.6%, while the positive contribution of $\langle -w\omega_y \rangle$ slightly increases about 7.0%. Under the intense negative and positive $u_L$ ($u_L^+ \le -2$ and $u_L^+ \ge +2$), the contribution of $\langle v\omega_z \rangle$ in the APG TBL is enhanced 8.33 and 2.72 times compared to the ZPG TBL. The skin friction induced by $\langle -w\omega_y \rangle$ increases 1.8 times only under $u_L^+ \ge +2$ in the APG TBL. The enhanced large-scale motions in the outer region strongly modulate the vortical motions. In particular, the low-speed structures augment the contribution of the advective vorticity transport and the contribution of the vortex stretching is enhanced under the influence of the high-speed structures in the APG TBL.

## INTRODUCTION

One of important features in APG TBLs is an increase of large scales in the outer region: e.g., a strong secondary peak in the pre-multiplied energy spectra of the streamwise velocity fluctuations (Harun *et al*. 2013; Lee 2017). Large-scale structures (LSSs), scale with $O(\delta)$, where $\delta$ is the boundary layer thickness, play an important role in the production of turbulent kinetic energy and the transport of momentum. LSSs contain about half of the turbulent kinetic energy and Reynolds shear stress in turbulent flows (Guala *et al*. 2006; Balakumar & Adrian 2007). LSSs with strong energy in the outer region extend to the near-wall region as footprints (Hutchins & Marusic 2007a). Hutchins & Marusic (2007b) observed that amplitudes of three velocity fluctuations and the Reynolds shear stress are attenuated under negative large-scale fluctuations at $y^+ = 15$ in the instantaneous fluctuating signals. To measure a degree of amplitude modulation (AM) influences, Mathis *et al*. (2009) introduced AM coefficient, which is the correlation between the large-scale fluctuations and filtered envelope of small-scale fluctuations. Using the AM coefficient, the AM influences of LSSs on small scales were investigated for the streamwise velocity fluctuations (Mathis *et al*. 2009) and for the cross-stream components (Talluru *et al*. 2014). Since the outer energy carried by the large scales is enhanced in APG TBLs, the degree of the AM for the streamwise components is enhanced compared to ZPG TBLs (Harun *et al*. 2013; Lee 2017).

Given that the footprints of large-scales low-speed structures is narrower than that of the low-speed structure (Hwang *et al*. 2016), the influence of outer large-scale low- and high-speed structures is asymmetric in the near-all region (Agostini & Leschziner 2014; Hwang *et al*. 2016). This difference is related to the near-wall spanwise motions induced by the associated large-scale circulations, which are congregative and dispersive (Hwang *et al*. 2016). Ganapathisubramani *et al*. (2012) statistically investigated the AM influences on the small-scale streamwise velocity fluctuations with respect to the strength of large scales and showed that the amplitude of the small scales in the near-wall region is attenuated or amplified under the negative of positive large scales, respectively. Since the near-wall vortical structures are related to the small-scale velocity fluctuations, the vortical motions could be affected by the outer large-scale structures and thus the large-scale influences on the vortical motions could be enhanced in APG TBLs.

Recently, Yoon *et al*. (2016a) derives an expression for the skin friction coefficient ($C_f$), which quantifies the contributions of the velocity-vorticity correlations ($\langle v\omega_z \rangle$ and $\langle -w\omega_y \rangle$) to the skin friction. The correlations $\langle v\omega_z \rangle$ and $\langle -w\omega_y \rangle$ are interpreted as the advective vorticity transport and vortex stretching (Tennekes & Lumley 1972). The streamwise vortical structures are a major part of the self-sustaining process since they create or amplify the near-wall streaks via the lift-up process (Kim 2011). Although the vortical motions play a crucial role in near-wall turbulence, most studies in the APG TBLs have not dealt with the influences of LSSs on the vortical motions. In the APG TBL, the streamwise

vortical motions ($y^+ < 50$) are inclined steeper and stronger than that in the ZPG TBL (Lee & Sung 2008). Given that the intensity of the inner peak in the streamwise energy spectra is unaffected by the pressure gradient (Harun *et al*. 2013), the relatively strong vortical motions could be related to the presence of the intense outer peak, leading to the enhanced influence of LSSs on the near-wall region in APG TBL. In the present study, therefore, we explore large-scale influences on the vortical motions, which ultimately contribute to the skin friction in the APG TBL. For comparison, DNS data of a ZPG TBL of Hwang & Sung (2017) are analyzed.

## NUMERICAL SIMULATION

The governing equations with non-dimensional form for an incompressible flow are

$$\frac{\partial \tilde{u}_i}{\partial t} + \frac{\partial \tilde{u}_i \tilde{u}_j}{\partial x_j} = -\frac{\partial \tilde{p}}{\partial x_i} + \frac{1}{Re}\frac{\partial}{\partial x_j}\frac{\partial \tilde{u}_i}{\partial x_j}, \quad (1)$$

$$\frac{\partial \tilde{u}_i}{\partial x_i} = 0, \quad (2)$$

where $x_i$ are the Cartesian coordinates and $\tilde{u}_i$ are the corresponding velocity components ($\tilde{u}_i \equiv U_i + u_i$). $x$, $y$, and $z$ denote the streamwise, wall-normal, spanwise coordinates, and $u$, $v$, and $w$ indicate the corresponding velocity fluctuations, respectively. The angle bracket represents ensemble-averaged quantities. Each term in the governing equations is normalized by inlet free-stream velocity ($U_0$) and inlet boundary layer thickness ($\delta_0$). The Reynolds number is defined as $Re = U_0\delta_0/\nu$, where $\nu$ is the kinematic viscosity. The pressure and velocity are decoupled by using fully implicit fractional step method to solve the governing equations. The second-order Crank-Nicolson scheme is used to discretize the convection and viscous terms in time implicitly. The second-order central difference scheme is used to discretize all terms in space with a staggered grid. Details of the numerical procedure can be found in Kim *et al.* (2002).

The inflow condition is imposed as a superposition of the Blasius velocity profile and isotropic free-stream turbulence. The free-stream turbulence is generated by the Orr–Sommerfeld and Squire modes in the wall-normal direction and Fourier modes in time and in the spanwise direction (Jacobs & Durbin 2001). The turbulent intensity of the free-stream turbulence is set to 5% and superimposed up to $2\delta_0$ in the inlet. Details of the inflow generation at TBLs and simulation setup for a ZPG TBL are shown in Hwang & Sung (2017). The boundary layer develops along a long domain from $Re_\theta$ ($= U_\infty\theta/\nu$) $\approx$ 108 extending up to $Re_\theta \approx 6000$, where $U_\infty$ is the free-stream velocity and $\theta$ is the momentum thickness. The periodic boundary condition is applied to the spanwise direction, and the no-slip boundary condition is imposed on the bottom wall. The convective boundary condition ($\partial\tilde{u}/\partial t + c\partial\tilde{u}/\partial x = 0$, where $c$ is local bulk velocity) is used at the exit, and the Neumann boundary condition ($\partial\tilde{u}/\partial y = \partial\tilde{w}/\partial y = 0$) is used in the upper boundary. Figure 1 represents the power-law distribution of the free-stream velocity, $U_\infty = U_0(1 - x/200\delta_0)^{-0.2}$, which is imposed on the Neumann boundary condition using the continuity, $\partial\tilde{v}/\partial y = -\partial U_\infty/\partial x$. The power-law distribution of $U_\infty$ is applied after $x/\delta_0 = 600$, representing that APG is activated after the transition to turbulence. Numerical details of the DNS are summarized in Table 1. The superscript + represents normalized quantities by the viscous scales, which were obtained at $Re_\tau = 834$ for both APG and ZPG TBLs, where $Re_\tau$ is the friction Reynolds number ($= u_\tau\delta/\nu$). The time step in the wall unit $\Delta t^+$ is 0.0744, and the total averaging time $t_{avg}$ is $6160\delta_0/U_0$. To perform the DNS of the APG TBL, hybrid parallel computing with OpenMP and MPI is employed in the code and the simulation is performed using 1024 cores of Tachyon II (SUN B6275) at the KISTI supercomputing center.

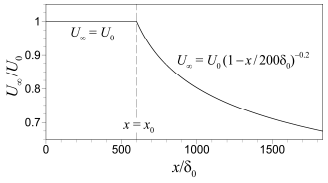


Figure 1. Power-law distribution of free-stream velocity.

Table 1. Parameters of the simulations. $L_i$ and $N_i$ are domain size and the number of grid in each direction. $\Delta x^+$ and $\Delta z^+$ are the grid resolutions in streamwise and spanwise directions, respectively. $\Delta y^+_{\min}$ and $\Delta y^+_{100}$ indicate the minimum grid resolution in wall-normal direction and the resolution of 100th grid from the wall.

| | $L_x/\delta_0$ | $L_y/\delta_0$ | $L_z/\delta_0$ | $N_x$ | $N_y$ | $N_z$ | $\Delta x^+$ | $\Delta z^+$ | $\Delta y^+_{\min}$ | $\Delta y^+_{100}$ |
|---|---|---|---|---|---|---|---|---|---|---|
| APG TBL | 1834 | 100 | 130 | 10497 | 541 | 1025 | 3.34 | 2.43 | 0.098 | 0.296 |
| ZPG TBL | 2300 | 100 | 100 | 13313 | 541 | 769 | 5.60 | 4.21 | 0.165 | 0.501 |

## TURBULENCE STATISTICS

The mean velocity profiles of the APG and ZPG TBLs are shown in figure 2(a), and DNS data (circle symbol) of a ZPG TBL by Schlatter and Örlü (2010) are added for comparison. Here, the friction Reynolds number for the APG and ZPG TBL is $Re_\tau \approx 830$ and the pressure gradient parameter ($\beta$) (Clauser 1954) of the APG is $\beta = 1.45$. Note that turbulence statistics in the present study is averaged over the region $x' = x_r \pm 0.5\delta$, where $x_r$ is the reference position. Near the wall, the mean velocity of the APG TBL satisfies the law of the wall ($U^+ = y^+$). The logarithmic law is shifted downward, which is generally observed in APG TBLs, and also the large wake region is observed above $y^+ > 300$ (Lee & Sung 2008; Monty *et al*. 2011; Harun *et al*. 2013; Gungor *et al*. 2016; Lee 2017).

Figure 2(b) exhibits the profiles of the streamwise turbulent. Due to strong wake in the outer region, the profile of $\langle uu \rangle$ in the APG TBL has a clear peak at $y^+ \approx 300$. The presence of the outer peak are one of the characteristic of APG TBLs as reported in previous studies (Skåre & Krogstad 1994; Lee & Sung 2008; Monty *et al*. 2011; Harun *et al*. 2013; Gungor *et al*. 2016; Kitsios *et al*. 2016; Lee 2017). In the APG TBL, the value of the outer peak in $\langle uu \rangle$ is two times higher than $\langle uu \rangle$ at $y^+ \approx 300$ in the ZPG TBL. In addition, the inner peak of $\langle uu \rangle$ at $y^+ \approx 15$ increases in the APG TBL.

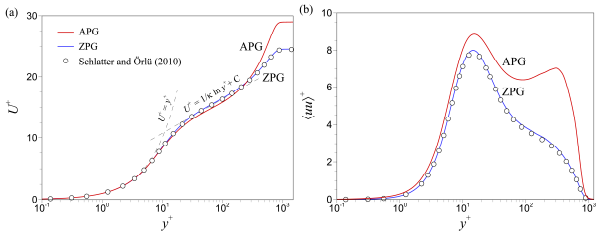


Figure 2. (a) Mean velocity profiles in the APG TBL at $Re_\tau = 834$ (red) and the ZPG TBL at $Re_\tau = 837$ (blue). Dashed lines indicate the law of the wall and the logarithmic law ($U^+ = 1/\kappa \ln y^+ + C$, where $\kappa$ is the von Kármán constant of 0.41 and $C$ is constant value of 0.51). (b) Profiles of the streamwise turbulent intensity in the APG and ZPG TBLs.

To further explore the contributions of scales to the difference in the streamwise turbulent intensity, one-dimensional pre-multiplied span-wise energy spectra of $uu$ ($k_z\phi_{uu}$) are introduced in figure 3. The $uu$-energy spectrum of the APG TBL shows that a strong peak in the outer region ($y^+ \approx 300$) results from the energy carried by the long wavelength ($\lambda_z^+ \approx 630$). The outer-peak value in the APG TBL increases by 174% than that in the ZPG TBL, representing that the LSSs are more energetic due to the presence of the APG. In the present study, the cut-off wavelength of $\lambda_{z,c}^+ = 400$ (dashed lines in figure 3), which is consistent with the cut-off wavelength $\lambda_{z,c}/\delta \approx 0.5$ (Bernardini & Pirozzoli 2011; Ahn *et al*. 2013; Hwang *et al*. 2017), is selected to decompose the streamwise velocity fluctuations into small and large scales. For the APG TBL, in addition, the energy in the inner region, related to the self-sustaining process of small scales (Hamilton *et al*. 1995), is slightly reduced in comparison to that of the ZPG TBL. As shown in figure 2(b), however, the inner peak of $\langle uu \rangle$ in the APG TBL is higher than that in the ZPG TBL, indicating that the superimposed large scales ($\lambda_z^+ > 400$) in the near-wall region (footprints) dominantly contributes to the increase of the inner peak of $\langle uu \rangle$ in the APG TBL. In other words, the enhanced LSSs in the outer region increases streamwise turbulent intensity not only in the outer region but also in the near-wall region, since the footprints of LSSs become dominant in the APG TBL. This result implies that the footprints of LSSs in the APG TBL could enhance the large-scale influence on the near-wall turbulence compared to those in the ZPG TBL. Furthermore, the $uu$ energy carried by the small-scale motions ($\lambda_z^+ < 400$) above $y^+ = 200$ increases in the APG TBL due to high production (Skåre & Krogstad 1994; Lee & Sung 2008; Harun *et al*. 2013; Kitsios *et al*. 2016).

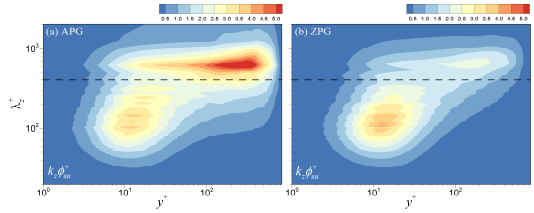


Figure 3. Pre-multiplied spanwise energy spectra of streamwise velocity fluctuations in (a) the APG TBL and (b) the ZPG TBL. Dashed line indicates the cut-off wavelength, $\lambda_{z,c}^+ = 400$.

## CONDITIONAL SAMPLING

In order to examine the amplitude modulation of the vortical structures in terms of the strength of LSSs, the procedure used in Ganapathisubramani *et al*. (2012) and Hwang & Sung (2017) is adopted for the conditional sampling the amplitudes of the vortical motions. Figure 4 shows sample signals at $y^+ = 15$ to explain the procedure for the conditional sampling method. First, long-wavelength streamwise velocity fluctuations ($u_L$) are separated from $u$ through the long-wavelength-pass filter with $\lambda_{z,c}^+ = 400$. Figure 4(a) illustrates the signals of $u$ (grey) and $u_L$ (black). Second, the fluctuating signals are divided into individual segments of length $400\delta^+$, which corresponds to the cut-off wavelength. Vertical dashed lines in this figure mark the district of each segment. Inserted circles in figure 4(a), which indicate values of $u_L^+$ at the center in each segment, denote the representative of $u_L$ in each segment. The bin size of $u_L^+$ in the conditional sampling of LSSs is set as 0.2 (Ganapathisubramani *et al*. 2012; Hwang & Sung 2017). Third, *rms* values of all signals are averaged at each segment as a function of $u_L$ and $y$.

The streamwise vorticity fluctuations at the same wall-normal location of $u$ and $u_L$ is shown in figure 4(b). Here, the inserted numbers are *rms* values of the streamwise vorticity fluctuations in each segment. Red and blue used in figure 4(b) indicate the positive-$u_L$ ($u_L^+ > 0$) and negative-$u_L$ ($u_L^+ < 0$) events, respectively. The *rms* values of the streamwise vorticity fluctuations ($\omega_{x,rms}$) under the negative $u_L$ (blue) are lower than those under the positive $u_L$ (red). The amplitude of $\omega_x$ at the positive $u_L$ is amplified while it is attenuated under the negative $u_L$, reminiscent of the attenuation of the streamwise vorticity fluctuations under the footprints of low-speed structures (Yoon *et al*. 2016b).

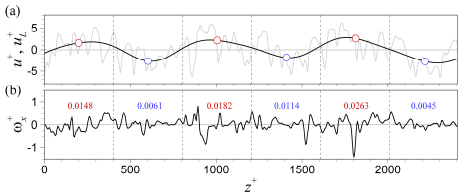


Figure 4. Signals of (a) streamwise velocity fluctuations (grey), long wavelength of $u$, and (b) streamwise vorticity fluctuations in the same wall-normal location in the APG TBL.

First of all, we investigate the population of $u_L$ using the probability density function (PDF), which is defined as $N(u_L, y)/\sum_{u_L} N(u_L, y)$, where $N(u_L, y)$ is the number of samples at certain $u_L$ and $y$. Figure 5(a,b) displays PDFs of $u_L$ in the APG and ZPG TBLs, respectively. Near the wall and boundary layer edge, high probability values are observed in the vicinity of $u_L^+ = 0$, representing a narrow distribution of $u_L$ because the fact that small-scale fluctuations are dominant in the near-wall region and near the boundary layer edge. Although the PDFs of $u_L$ for both TBLs have a peak in the vicinity of $u_L^+ = 0$ and decrease with an increase in $|u_L^+|$, the PDF of the APG TBL is widely distributed with relatively higher magnitude of $|u_L^+|$ than that of the ZPG TBL. Moreover, PDFs of $u_L$ are not symmetric along $u_L^+ = 0$; in other

words, the population of $u_L$ is biased toward a negative $u_L$ or positive $u_L$ at certain wall-normal location. As shown in figure 5(a), high-speed LSSs with $u_L^+ = +6$ are observed near $y^+ = 200$, where low-speed LSSs with $u_L^+ = -6$ are not observed, and vice versa near $y^+ = 400$. Figure 5(c) denotes averaged PDF of $u_L$ from $y^+ = 15$ to 400, where PDF of $u_L$ for both TBLs are symmetric with respect to $u_L^+ = 0$. Vertical dashed lines in figure 5(c) mark $u_L^+ = \pm 2$, where the PDF of $u_L$ is half of value at $u_L^+ = 0$ in both flows. Interestingly, the PDFs of $u_L$ cross at $u_L^+ = \pm 2$, indicating that the intense low- and high-speed $u_L$ ($u_L^+ \le -2$ and $u_L^+ \ge +2$) frequently occur in the APG TBL, whereas the relatively weak $u_L$ ($-2 \le u_L^+ \le +2$) decreases. The higher values of PDF for $u_L^+ \le -2$ and $u_L^+ \ge +2$ contribute to the increase of outer large-scale energy in the pre-multiplied spanwise energy spectra of $uu$ (figure 3).

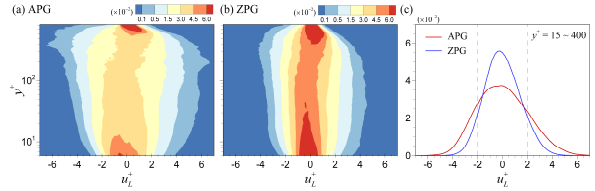


Figure 5. Population of long-wavelength $u$ ($u_L$) with respect to the wall-normal location and strength of $u_L$ in (a) the APG TBL and (b) the ZPG TBL. (c) Averaged profiles from $y^+ = 15$ to 400 of population of $u_L$ in the APG TBL and the ZPG TBL. Vertical dashed lines indicate $u_L^+ = \pm 2$.

## LARGE-SCALE INFLUENCES ON SKIN FRICTION

In this section, we investigate the large-scale influence on the velocity-vorticity correlations, which are directly related to the skin friction coefficient (Yoon *et al.* 2016a). Applying the triple integration on the spanwise component of the mean vorticity equation, the skin friction coefficient ($C_f$) can be decomposed into four terms as follows

$$C_f = \underbrace{2\int_0^1 (1-y/\delta)\langle v\omega_z\rangle \mathrm{d}\frac{y}{\delta}}_{C_{f,1}} + \underbrace{2\int_0^1 (1-y/\delta)\langle -w\omega_y\rangle \mathrm{d}\frac{y}{\delta}}_{C_{f,2}} + \underbrace{\frac{1}{Re}\frac{\partial \Omega_z}{\partial y}\bigg|_{y=0} - \frac{2}{Re}\int_0^1 \Omega_z \mathrm{d}\frac{y}{\delta} + \int_0^1 (1-y/\delta)^2 \langle I_x\rangle \mathrm{d}\frac{y}{\delta}}_{C_{f,\mathrm{others}}}, \quad (4)$$

where $Re$ is defined as $\delta U_\infty/\nu$ and $\langle I_x\rangle = \partial(U\Omega_z + \langle u\omega_z\rangle - \langle w\omega_x\rangle)/\partial x + \partial(V\Omega_z)/\partial y - Re^{-1}\partial^2\Omega_z/\partial x^2$ is a streamwise-inhomogeneous term. The first and second terms ($C_{f,1}$ and $C_{f,2}$) represent the contributions of the advective vorticity transport $\langle v\omega_z\rangle$ and of the vorticity stretching $\langle -w\omega_y\rangle$ (Tennekes & Lumley 1972) to the skin friction, respectively.

Figure 6 represents the decomposition of the skin friction coefficient using equation (4) in the APG and ZPG TBLs. As shown in figure 6, $C_{f,1}$ and $C_{f,2}$ constitute the majority of the total $C_f$. Accordingly, we focus on $C_{f,1}$ and $C_{f,2}$ in the present study. In the APG TBL, the magnitude of $C_{f,1}$ which reduces the total $C_f$, decreases, while the value of $C_{f,2}$, which enhance the total $C_f$, increases compared to those in the ZPG TBL. The variation of $C_{f,1}$ and $C_{f,2}$ in the APG TBL augments the total $C_f$ but the total $C_f$ in the APG TBL is lower than that in the ZPG TBL due to the negative contribution of $C_{f,\mathrm{others}}$.

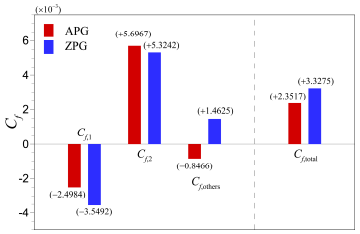


Figure 6. Decomposition of the skin-friction coefficients in the APG TBL and the ZPG TBL.

To investigate the influences of LSSs on $C_{f,1}$ and $C_{f,2}$, two velocity-vorticity correlations ($\langle v\omega_z\rangle$ and $\langle -w\omega_y\rangle$) are conditionally averaged as a function of $u_L$ and $y$,

$$\langle v\omega_z|u_L\rangle = \langle \Sigma v\omega_z|u_L\rangle / N_{u_L}(u_L, y),$$
$$\langle -w\omega_y|u_L\rangle = \langle \Sigma -w\omega_y|u_L\rangle / N_{u_L}(u_L, y), \quad (5)$$

and then the contribution of the modulated vortical motions $\langle C_{f,1}|u_L\rangle$ and $\langle C_{f,2}|u_L\rangle$ can be obtained through the integration of equations (5),

$$\langle C_{f,1}|u_L\rangle = \int_0^1 \underbrace{2y(1-y/\delta)\langle v\omega_z|u_L\rangle}_{=\zeta_{f,1}(u_L,y)} \mathrm{d}\ln\frac{y}{\delta},$$
$$\langle C_{f,2}|u_L\rangle = \int_0^1 \underbrace{2y(1-y/\delta)\langle -w\omega_y|u_L\rangle}_{=\zeta_{f,2}(u_L,y)} \mathrm{d}\ln\frac{y}{\delta}. \quad (6)$$

Hence, the summation of $\langle C_{f,i}|u_L\rangle$ along all $u_L$ is the same as value $C_{f,i}$ in figure 6 $\sum_{u_L}\langle C_{f,i}|u_L\rangle = C_{f,i}$ ($i$ = 1, 2).

Figure 7 displays 2D contour plot of $\zeta_{f,1}(u_L, y)$ and $\zeta_{f,2}(u_L, y)$, which directly indicate the contribution of the advective vorticity transport and the vortex stretching influenced by the strength of $u_L$. In $\zeta_{f,1}(u_L, y)$ on the left of figure 7, a positive value below $y/\delta$ = 0.01 near $u_L^+ = 0$, which is considered as the unmodulated signals, in the APG TBL decreases compared to that in the ZPG TBL. At that region, $\langle v\omega_z\rangle$ related with $\zeta_{f,1}(u_L, y)$ physically represents that lifting sublayer streaks (Klewicki *et al.* 1994; Chin *et al.* 2014) is weakened in the APG TBL, where Lee & Sung (2009) show a diminution of the sublayer streaks through the flow visualization of $u$ at $y^+ = 5.5$. Between $y/\delta = 0.1$ and 0.01, a negative $\zeta_{f,1}(u_L, y)$ near $u_L^+ = 0$ decreases in the APG TBL more than that in the ZPG TBL. At that region, $\langle v\omega_z\rangle$ is well-known as lifting the hairpin vortex heads (Klewicki *et al.* 1994;

Chin *et al.* 2014), which could be weakened in the APG TBL. Above $y/\delta = 0.1$, furthermore, the influences of $u_L^+ \le -2$ and $u_L^+ \ge +2$ on $\zeta_{f,1}(u_L, y)$ increase substantially in the APG TBL.

On the right of figure 7, a positive value of $\zeta_{f,2}(u_L, y)$ near $u_L^+ = 0$ is reduced in the APG TBL compared to the ZPG TBL below $y/\delta = 0.02$. At that region, $\langle -w\omega_y \rangle$ related with $\zeta_{f,2}(u_L, y)$ physically represents a simultaneous collapse of two adjacent hairpin vortex legs inducing the vortex stretching (Eyink 2008; Chin *et al.* 2014). Above $y/\delta = 0.02$, however, a positive $\zeta_{f,2}(u_L, y)$ under $u_L^+ \ge +2$ increases significantly in the APG TBL, which results in larger $C_{f,2}$ in the APG TBL (figure 6). In the APG TBL, the high-speed LSSs in the outer region amplified the vortical motions of $\langle -w\omega_y \rangle$ resulting in an increase of $C_{f,2}$.

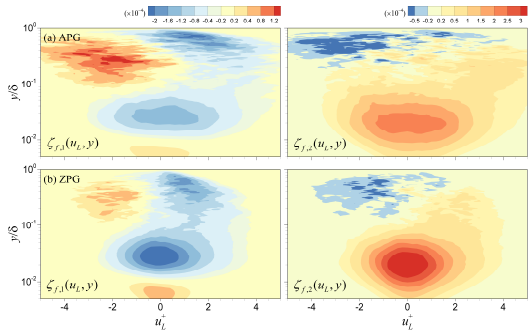


Figure 7. Integrands of $\langle C_{f,1}|u_L \rangle$ and $\langle C_{f,1}|u_L \rangle$, which are $\zeta_{f,1}(u_L, y)$ and $\zeta_{f,1}(u_L, y)$, with semi-log scale at wall-normal direction in (a) the APG TBL and (b) the ZPG TBL

Figure 8(a,b) shows the profiles of $\langle C_{f,1}|u_L \rangle$ and $\langle C_{f,2}|u_L \rangle$, and their cumulative distributions $\sum\langle C_{f,i}|u_L \rangle = \sum_{u_L^+=-\infty}^{u_L^+} \langle C_{f,i}|u_L \rangle$ are shown in figure 8(c,d). Although the total $C_{f,1}$ is negative, the contribution $\langle C_{f,1}|u_L \rangle$ for $u_L^+ < -2$ is positive in figure 8(a), indicating that $\langle v\omega_z \rangle$ under the low-speed LSSs enhances the skin friction while that under the high-speed LSSs ($u_L^+ > +2$) dominantly contributes to the reduction of the skin friction. The positive peak at $u_L^+ = -3$ in the APG TBL is two times larger than that in the ZPG TBL. In addition, the magnitude of the negative peak at $u_L^+ = +1.5$ is diminished in the APG TBL due to the enhancement of the positive region in the outer region as shown in figure 7(a). At $u_L^+ = -2$, the value of the cumulative distribution $\sum\langle C_{f,1}|u_L \rangle$ in the APG TBL is 8.3 times larger than that in the ZPG TBL (figure 8(c)). At $u_L^+ = +2$, $\sum\langle C_{f,1}|u_L \rangle$ is a half of the total $C_{f,1}$ in the APG TBL, which is 2.72 times larger than that in the ZPG TBL.

In figure 8(b), a larger value of $C_{f,2}$ occurs under $u_L^+ < -2$ and $u_L^+ > +2$ in the APG TBL and in particular the difference in $C_{f,2}$ is prominent under the positive $u_L$. The variation of $\sum\langle C_{f,2}|u_L \rangle$ under the low-speed LSSs is insignificant as shown in figure 8(d). At $u_L^+ = +2$, on the other hand, the value of $\sum\langle C_{f,2}|u_L \rangle$ is in the APG TBL 1.75 times larger than that in the ZPG TBL. In sum, in the APG TBL, the enhanced large-scale motions in the outer region strongly modulate the vortical motions, which ultimately contribute to the dependence of the skin friction. The influences of the low-speed LSSs ($u_L^+ < -2$) on $\langle C_{f,1}|u_L \rangle$ and of the high-speed LSSs ($u_L^+ > +2$) on $\langle C_{f,2}|u_L \rangle$ increase considerably in the APG TBL.

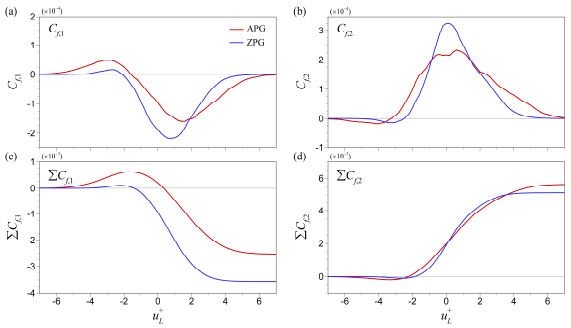


Figure 8. Profiles of (a) $\langle C_{f,1}|u_L \rangle$, (b) $\langle C_{f,2}|u_L \rangle$, (c) $\sum\langle C_{f,1}|u_L \rangle$, and (d) $\sum\langle C_{f,2}|u_L \rangle$ in the APG TBL and the ZPG TBL.

## CONCLUSIONS

We examine the influences of large-scale structures on the vortical motions in an APG TBL, which is performed by using the DNS and developed up to $Re_\theta = 6000$. In the present study, flow data of the APG TBL at $Re_\tau = 834$ and $\beta = 1.45$ are analyzed, and data of the ZPG TBL ($Re_\tau = 837$) are compared. Long-wavelength streamwise velocity fluctuations ($u_L$) are separated from raw signals of $u$ using the long-wavelength-pass filter with the cut-off wavelength $\lambda_{z,c}^+ = 400$. Using the conditional sampling methods, segments with $u_L^+ \le -2$ and $u_L^+ \ge +2$ are classified into the low- and high-speed LSSs, respectively. Two velocity-vorticity correlations ($\langle v\omega_z \rangle$ and $\langle -w\omega_y \rangle$) are directly related with the skin friction coefficient ($C_f$) (Yoon *et al.* 2016a) and indicate the advective vorticity transport and vortex stretching, respectively (Tennekes & Lumley 1972). The total $C_f$ in the APG TBL is 28% lower than that in the ZPG TBL. The skin friction induced by $\langle v\omega_z \rangle$ and $\langle -w\omega_y \rangle$ contribute negatively and positively to the total $C_f$, respectively. In the APG TBL, the negative contribution of $\langle v\omega_z \rangle$ increases 29.6%, while the positive contribution of $\langle -w\omega_y \rangle$ slightly increases about 7.0%. The correlations $\langle v\omega_z \rangle$ and $\langle -w\omega_y \rangle$ are conditionally averaged with respect to $u_L$ to extend the influences of the low- and high-speed LSSs on the vortical motions into the skin friction. Under the intense negative and positive $u_L$ ($u_L^+ \le -2$ and $u_L^+ \ge +2$), the contribution of $\langle v\omega_z \rangle$ in APG TBL is enhanced 8.3 and 2.7 times compared to that in ZPG TBL. Above $y/\delta = 0.1$, the contribution of $\langle v\omega_z \rangle$ under $u_L^+ \le -2$ and $u_L^+ \ge +2$ to the skin friction increases substantially in the APG TBL. The skin friction induced by

$\langle -w\omega_y \rangle$ increases 1.8 times only under $u_L^+ \geq +2$ in the APG TBL. Above $y/\delta$ = 0.02, the positive contribution of $\langle -w\omega_y \rangle$ under $u_L^+ \geq +2$ increases significantly in the APG TBL. The enhanced LSSs in the outer region strongly modulate the vortical motions. In particular, the low-speed LSSs augment the contribution to the skin friction induced by $\langle v\omega_z \rangle$, and the high-speed LSSs enhanced the contribution to that induced by $\langle -w\omega_y \rangle$ in the APG TBL.

## ACKNOWLEDGEMENT

This work was supported by the Creative Research Initiatives (No. 2017-013369) program of the National Research Foundation of Korea (MSIP), and partially supported by the Supercomputing Center (KISTI).

## REFERENCES

Agostini, L., and Leschziner, M. A., 2014, "On the influence of outer large-scale structures on near-wall turbulence in channel flow", *Physics of Fluids*, Vol. 26(7), 075107.

Ahn, J., Lee, J. H., Jang, S. J., and Sung, H. J., 2013, "Direct numerical simulations of fully developed turbulent pipe flows for $Re_\tau$ = 180, 544 and 934", *International Journal of Heat and Fluid Flow*, Vol. 44, pp. 222–228.

Balakumar, B. J., and Adrian, R. J., 2007, "Large-and very-large-scale motions in channel and boundary-layer flows", *Philosophical Transactions of the Royal Society of London A: Mathematical, Physical and Engineering Sciences*, Vol. 365(1852), pp. 665–681.

Bernardini, M., and Pirozzoli, S., 2011, "Inner/outer layer interactions in turbulent boundary layers: a refined measure for the large-scale amplitude modulation mechanism", *Physics of Fluids*, Vol. 23(6), 061701.

Chin, C., Philip, J., Klewicki, J., Ooi, A., and Marusic, I., 2014, "Reynolds-number-dependent turbulent inertia and onset of log region in pipe flows", *Journal of Fluid Mechanics*, Vol. 757, pp. 747–769.

Clauser, F. H., 1954, "Turbulent Boundary Layers in Adverse Pressure Gradients", *Journal of the Aeronautical Sciences*, Vol. 21(2), pp. 91–108.

Eyink, G. L., 2008, "Turbulent flow in pipes and channels as cross-stream "inverse cascades" of vorticity", *Physics of Fluids*, Vol. 20(12), 125101.

Ganapathisubramani, B., Hutchins, N., Monty, J. P., Chung, D., and Marusic, I., 2012, "Amplitude and frequency modulation in wall turbulence", *Journal of Fluid Mechanics*, Vol. 712, pp. 61–91.

Guala, M., Hommema, S. E., and Adrian, R. J., 2006, "Large-scale and very-large-scale motions in turbulent pipe flow", *Journal of Fluid Mechanics*, Vol. 554, pp. 521–542.

Gungor, A. G., Maciel, Y., Simens, M. P., and Soria, J., 2016, "Scaling and statistics of large-defect adverse pressure gradient turbulent boundary layers", *International Journal of Heat and Fluid Flow*, Vol. 59, pp. 109–124.

Hamilton, J. M., Kim, J., and Waleffe, F., 1995, "Regeneration mechanisms of near-wall turbulence structures", *Journal of Fluid Mechanics*, Vol. 287, pp. 317–348.

Harun, Z., Monty, J. P., Mathis, R., and Marusic, I., 2013, "Pressure gradient effects on the large-scale structure of turbulent boundary layers", *Journal of Fluid Mechanics*, Vol. 715, pp. 477–498.

Hutchins, N., and Marusic, I., 2007a, "Evidence of very long meandering features in the logarithmic region of turbulent boundary layers", *Journal of Fluid Mechanics*, Vol. 579, pp. 1-28.

Hutchins, N., and Marusic, I., 2007b, "Large-scale influences in near-wall turbulence", *Philosophical Transactions of the Royal Society of London A: Mathematical, Physical and Engineering Sciences*, Vol. 365(1852), pp. 647–664.

Hwang, J., Lee, J., Sung, H. J., and Zaki, T. A., 2016, "Inner-outer interactions of large-scale structures in turbulent channel flow", *Journal of Fluid Mechanics*, Vol. 790, pp. 128–157.

Hwang, J., and Sung, H. J., 2017, "Influence of large-scale motions on the frictional drag in a turbulent boundary layer", *Journal of Fluid Mechanics*, under review.

Jacobs, R. G., and Durbin, P. A., 2001, "Simulations of bypass transition", *Journal of Fluid Mechanics*, Vol. 428, pp. 185–212.

Kim, K., Baek, S. J., and Sung, H. J., 2002, "An implicit velocity decoupling procedure for the incompressible Navier–Stokes equations", *International journal for numerical methods in fluids*, Vol. 38(2), pp. 125-138.

Kitsios, V., Atkinson, C., Sillero, J. A., Borrell, G., Gungor, A. G., Jiménez, J., and Soria, J., 2016, "Direct numerical simulation of a self-similar adverse pressure gradient turbulent boundary layer", *International Journal of Heat and Fluid Flow*, Vol. 61, pp. 129–136.

Klewicki, J. C., Murray, J. A., and Falco, R. E., 1994, "Vortical motion contributions to stress transport in turbulent boundary layers", *Physics of Fluids*, Vol. 6(1), pp. 277–286.

Lee, J. H., 2017, "Large-scale motions in turbulent boundary layers subjected to adverse pressure gradients", *Journal of Fluid Mechanics*, Vol. 810, pp. 323–361.

Lee, J. H., and Sung, H. J., 2008, "Effects of an adverse pressure gradient on a turbulent boundary layer", *International Journal of Heat and Fluid Flow*, Vol. 29(3), pp. 568–578.

Lee, J. H., and Sung, H. J., 2009, "Structures in turbulent boundary layers subjected to adverse pressure gradients", *Journal of Fluid Mechanics*, Vol. 639, pp. 101–131.

Mathis, R., Hutchins, N., and Marusic, I., 2009, "Large-scale amplitude modulation of the small-scale structures in turbulent boundary layers", *Journal of Fluid Mechanics*, Vol. 628, pp. 311-337.

Monty, J. P., Harun, Z., and Marusic, I., 2011, "A parametric study of adverse pressure gradient turbulent boundary layers", *International Journal of Heat and Fluid Flow*, Vol. 32(3), pp. 575–585.

Schlatter, P., and Örlü, R., 2010, "Assessment of direct numerical simulation data of turbulent boundary layers", *Journal of Fluid Mechanics*, Vol. 659, pp. 116–126.

Skåre, P. E., and Krogstad, P. Å., 1994, "A turbulent equilibrium boundary layer near separation", *Journal of Fluid Mechanics*, Vol. 272, pp. 319–348.

Talluru, K. M., Baidya, R., Hutchins, N., and Marusic, I., 2014, "Amplitude modulation of all three velocity components in turbulent boundary layers", *Journal of Fluid Mechanics*, Vol. 746, R1.

Tennekes, H., and Lumley, J. L., 1972, *A first course in turbulence*. MIT press.

Yoon, M., Ahn, J., Hwang, J., and Sung, H. J., 2016a, "Contribution of velocity-vorticity correlations to the frictional drag in wall-bounded turbulent flows", *Physics of Fluids*, Vol. 28(8), 081702.

Yoon, M., Hwang, J., Lee, J., Sung, H. J., and Kim, J., 2016b, "Large-scale motions in a turbulent channel flow with the slip boundary condition", *International Journal of Heat and Fluid Flow*, Vol. 61, pp. 96–107.

Zhou, J., Adrian, R. J., Balachandar, S., and Kendall, T. M., 1999, "Mechanisms for generating coherent packets of hairpin vortices in channel flow", *Journal of Fluid Mechanics*, Vol. 387, pp. 353–396.